THE JOURNAL OF PHYSICAL CHEMISTRY C
A JOURNAL OF THE AMERICAN CHEMICAL SOCIETY

pubs.acs.org/JPCC

Article

# Identifying Practical DFT Functionals for Predicting 0D and 1D Organic Metal-Halide Hybrids

Yufang He, Md Sazedul Islam, Jarek Viera, Hanwei Gao, Jianwei Sun, Biwu Ma,* and Bin Ouyang*

Cite This: *J. Phys. Chem. C* 2024, 128, 17850−17858

Read Online

ACCESS | Metrics & More | Article Recommendations | Supporting Information

**ABSTRACT:** Low-dimensional organic metal-halide hybrids (LD-OMHHs) are a promising class of materials for applications in optical, magnetic, and quantum information technologies. Computational understanding of these materials necessitates reliable and efficient methods for property prediction, such as predicting the electronic band gap. This work systematically benchmarks three density functional theory (DFT) functionals as well as the impact of spin−orbital coupling on the band gap predictions for 110 experimentally reported LD-OMHHs. Surprisingly, the band gap predicted by the generalized gradient approximation (GGA) aligns similarly or better with experimentally measured values compared to two meta-GGA methods. Furthermore, spin−orbital coupling shows a limited impact on these predictions. The potential existence of significant excitonic effects might explain the discrepancies between meta-GGA and experimental band gaps. Our research also reveals that the direct use of the GGA functional can already be practical and efficient for high-throughput screening of LD-OMHHs with reasonable band gaps.

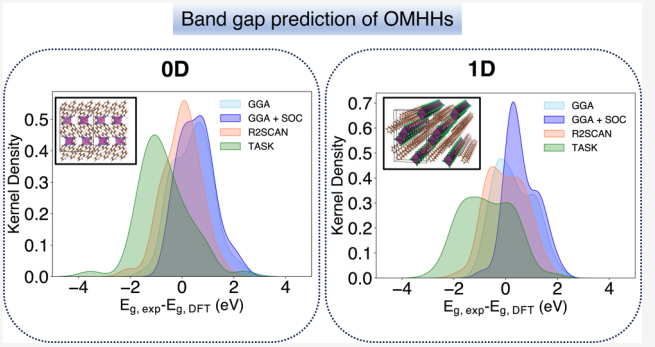




## 1. INTRODUCTION

Low-dimensional organic metal-halide hybrids (LD-OMHHs)[1−4] have recently been developed as versatile material platforms with applications in various types of optoelectronic devices, such as photovoltaic cells (PVs), light-emitting diodes (LEDs), and photodetectors for their unique and remarkable optical and electronic properties.[5−8] Unlike conventional perovskite structures with metal-halide polyhedra connecting to form 3D frameworks, LD-OMHHs contain anionic metal-halide species isolated and surrounded by organic cations, forming 2D, 1D, and 0D structures at the molecular level.[9,10] Due to the site isolation and quantum confinement effects, LD-OMHHs exhibit distinct properties as compared to their 3D perovskites. For instance, the corrugated 2D- and 1D-OMHHs with electronic band formation and structural distortions exhibit broadband emissions from a combination of direct and self-trapped excited states, producing near-white emissions.[4,11,12] 0D-OMHHs without electronic band formation show broadband emissions from the reorganized excited states, with high photoluminescence quantum efficiencies (PLQEs) of up to 100%.[3,13−16]

Accurate prediction of properties of such OMHHs urges a systematic benchmark against experimental results. Among all of these applications, one common purpose for theoretical computation is to predict the band structure and band gap. However, which DFT functional is optimal for exploring and predicting the band gap of LD-OMHH systems remains uncertain. In this work, we have conducted a systematic evaluation of the prediction power of different DFT functionals in terms of band gap prediction for LD-OMHHs, in particular, 0D and 1D ones. The experimental band gaps of 56 0D-OMHHs and 54 1D-OMHHs are extracted from the literature to serve as the "ground truth" of our prediction. Four types of DFT setups, generalized gradient approximation (GGA), GGA with spin−orbital coupling (denoted as GGA+SOC), R2SCAN, and TASK, are benchmarked against the 110 OMHHs. Specifically, R2SCAN is shown as a low-scaling meta-GGA method[17] that is able to offer an accurate prediction of both formation enthalpy and band gaps.[18−21] On the other hand, TASK has emerged as a meta-GGA method that has lower computing cost than hybrid functionals but offers similar performance in terms of predicting band gaps for perovskite and perovskite-related materials.[22,23] Surprisingly, we have found that the GGA level of theory outperforms TASK and gets very close to R2SCAN in terms of predicting band gaps for 0D- and 1D-OMHHs. Given that it is well known in the field of DFT that semilocal methods such as GGA will always underestimate the band gap,[22,24,25] our

**Received:** August 5, 2024
**Revised:** September 29, 2024
**Accepted:** October 7, 2024
**Published:** October 15, 2024

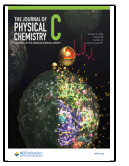





https://doi.org/10.1021/acs.jpcc.4c05263
*J. Phys. Chem. C* 2024, 128, 17850−17858

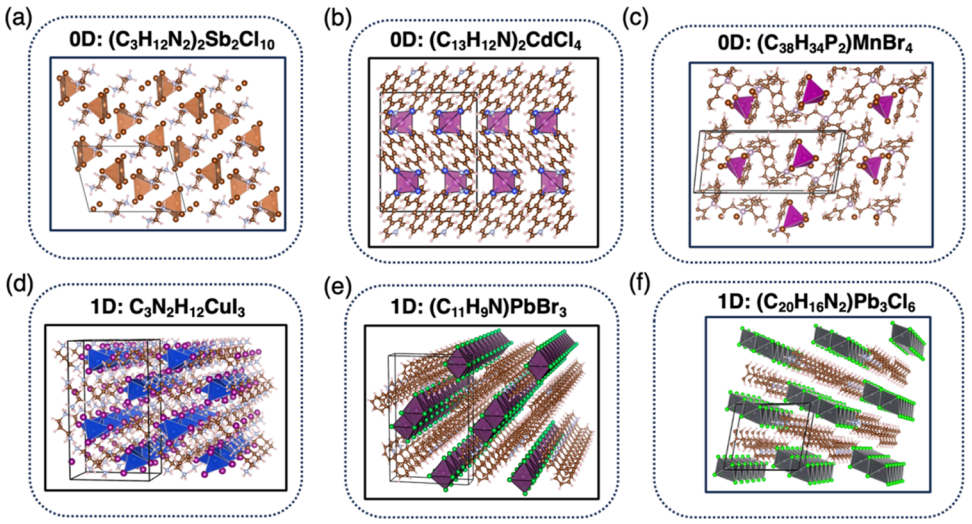


**Figure 1.** Representative atomic structures of 0D- and 1D-OMHHs: (a) 0D-$(C_3H_{12}N_2)_2Sb_2Cl_{10}$, (b) 0D-$(C_{13}H_{12}N)_2CdCl_4$, (c) 0D-$(C_{38}H_{34}P_2)MnBr_4$, (d) 1D-$C_3N_2H_{12}CuI_3$, (e) 1D-$(C_{11}H_9N)PbBr_3$, and (f) 1D-$(C_{20}H_{16}N_2)Pb_3Cl_6$.

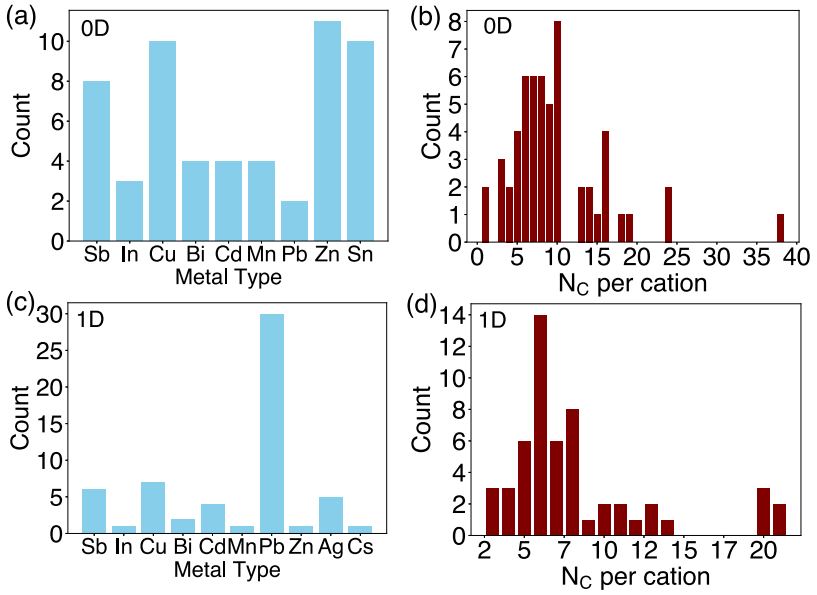


**Figure 2.** Chemical spaces of examined 0D- and 1D-OMHHs: (a) metal species and (b) number of carbon atoms per organic cation (denoted as $N_c$ per cation) of 0D-OMHHs; (c) metal species and (d) $N_c$ per cation of 1D-OMHHs.

unexpected observations reveal that there could be unprecedented excitonic effects in such systems, which make the DFT-predicted band gap differ a lot from the optical band gap. Nevertheless, our analysis indicates that GGA by itself will be useful to massively screen down OMHHs with appropriate optical band gaps, while a more physically insightful investigation may be needed for a short list of materials by combining the hyper-GGA level of theory or beyond with experimental measurement of the excitonic effect.[25]

## 2. METHODOLOGY

To investigate the electronic properties of 0D- and 1D-OMHHs, density functional theory (DFT) calculations were carried out using the Vienna ab initio simulation package (VASP)[26] and the projector-augmented wave (PAW) method.[27,28] A reciprocal mesh discretization of 25 $Å^{-1}$ was used for each calculation. Both lattice parameters and atomic positions were relaxed in DFT calculations. The convergence criteria were set to $10^{-6}$ eV for electronic iterations and 0.05 eV/Å for ionic iterations. Such a convergence criterion has been tested to give neglectable energy difference compared to a much stricter accuracy setup. A Gaussian-type smearing of the Fermi level was applied. A plane-wave energy cutoff of 520 eV was used for all of the calculations. All structural optimizations were done with GGA before applying different methods for band structure calculations.

Many 0D and 1D-OMHHs have large unit cells of more than 100 atoms, and in some cases larger than 500 atoms. It is possible to calculate a few band structures with higher-level theory, such as hybrid functionals, GW, random-phase approximation, Quantum Monte Carlo,[29−34] etc. However, given the extremely high cost of doing high-throughput screening with such functionals, we have tested only four small systems of 0D- and 1D-OMHHs using HSE06 and regard the use of hyper-GGA or higher-level theory as impractical for large-scale screening of OMHHs.



https://doi.org/10.1021/acs.jpcc.4c05263
J. Phys. Chem. C 2024, 128, 17850−17858

## 3. RESULTS

**3.1. Coverage of Chemical Spaces of OMHHs.** The atomic structures of 56 zero-dimensional (0D) OMHHs and 54 one-dimensional (1D) OMHHs have been obtained from the experimental literature. Three representative atomic structures for both 0D- and 1D-OMHHs are displayed in Figure 1. The organic cations in compounds $(C_3H_{12}N_2)_2Sb_2Cl_{10}$, $(C_{13}H_{12}N)_2CdCl_4$, and $(C_{38}H_{34}P_2)MnBr_4$ have been selected to exemplify the 0D-OMHHs, which vary in the amount of carbon per organic cations, as shown in Figure 1(a)−1(c). Similarly, $C_3N_2H_{12}CuI_3$, $(C_{11}H_9N)PbBr_3$, and $(C_{20}H_{16}N_2)Pb_3Cl_6$ have been chosen to represent the 1D-OMHHs, which differ in the size of the organic cations based on the carbon content, as depicted in Figure 1(d)−(f). This also clarifies that the terms 0D and 1D refer to the connectivity topology of the metal-halide polyhedra (Figure 1). Specifically, 0D-OMHHs contain isolated metal-halide polyhedra periodically interspersed with organic cations, whereas 1D-OMHHs consist of a one-dimensional periodic chain of metal-halide motifs.

Additionally, the compositional space of our examined compounds is demonstrated in Figure 2. Particularly, 56 0D-OMHHs and 54 1D-OMHHs are obtained from the existing literature. The coverage of chemical spaces can be demonstrated by the histogram shown in Figure 2. These compounds are grouped based on the metal species as well as the number of carbon atoms of each organic cations (denoted as $N_c$ per cations in Figure 2(b) and 2(d)). It can be inferred from Figure 2(a) and Figure 2(c) that the band gaps of 0D-OMHHs reported experimentally are more diverse in metals, while around 55.56% of 1D-OMHHs are Pb-containing compounds, in contrast to only 3.57% of Pb-containing compounds in the case of 0D-OMHHs. Moreover, it can also be inferred from Figure 2(b),(d) that 0D-OMHHs, in general, accommodate larger cations with more carbon; this can be represented by compounds that have more than 21 C atoms per cation for 0D-OMHHs as shown in Figure 2(b), which is absent for 1D cases shown by Figure 2(d). Some of the representative 0D-OMHHs with large organic cations can be represented by $(C_{38}H_{34}P_2)MnBr_4$ with $(C_{38}H_{34}P_2)^+$ as the organic cation,[35] $C_{24}H_{20}PCuBr_2$ with $(C_{24}H_{20}P)^+$ as the organic cation, as well as $(C_{24}H_{20}P)_2Cd_2Br_6$ with $(C_{24}H_{20}P)^+$ as the organic cation. Such a distribution of cation size can be understood as the fact that there is much less topological constraint for 0D-OMHHs as the metal-halide polyhedron does not need to connect in a way to maintain the periodicity of the inorganic motif in any dimension.

**3.2. Comparison among GGA, R2SCAN, and TASK.** With the establishment of all data sets, we then computed the band structure using three types of functionals: GGA, R2SCAN, and TASK. GGA is the most widely used functional and offers a reasonable estimation of material properties in many situations.[36] On the other hand, R2SCAN[17,37,38] emerged recently as a low-scaling meta-GGA method that offered improved accuracy for many properties, such as formation enthalpy, decomposition energy, as well as mechanical properties. Last but not least, TASK was also selected for comparison as it was recently reported to be functional and capable of predicting the band gap with similar behavior to the HSE level of hybrid functionals but with much less cost.[22] It is also reported that TASK offers a better prediction of the band gap of halide perovskites, which is a chemical system close to that of the material systems discussed in this work.

The parity plot of the experimental band gap versus DFT computed band gap using different functionals is demonstrated in Figure 3. The band gap values of experimental, GGA, R2SCAN, and TASK for 0D- and 1D-OMHHs are listed in Tables S1 and S2. Here, 0D-OMHHs and 1D-OMHHs are separated to check whether the dimensionality of the metal-halide bond topology will play a role in the prediction accuracy. Several interesting observations can be made from Figure 3. Particularly, R2SCAN tends to show the best prediction accuracy among the three functionals for both 0D- and 1D-OMHHs. However, the mean absolute error (MAE) predictions from R2SCAN are quite close to those from GGA, with a slight difference of 0.16 eV for the 0D case versus 0.03 eV for the 1D case. On the other hand, TASK tends to mostly overestimate the band gap with the MAE values being 0.99 eV for 0D cases and 0.98 eV for 1D cases, which is 0.31 and 0.33 eV larger than the GGA prediction. The observation for band gap prediction from TASK is also consistent with the fact that the HSE level of theory tends to predict a larger band gap than the GGA level of theory,[39−42] particularly considering that TASK is claimed to be able to match HSE band structure prediction with much lower computing cost.[22] On the other hand, both R2SCAN and TASK tend to predict larger band gap values than GGA in general. This is also consistent with the typical understanding that GGA tends to underestimate band gaps compared to other DFT methods.[17,24,37,43,44]

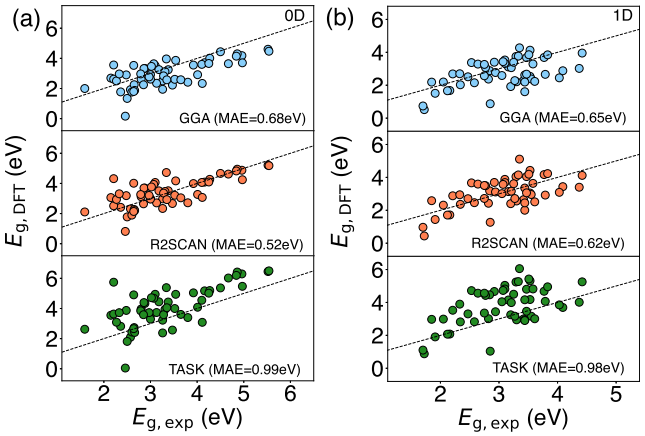


**Figure 3.** Comparison of band gap estimation of (a) 0D- and (b) 1D-OMHHs from GGA, R2SCAN, and TASK with the experimental band gap reported in the literature.

In addition to Figure 3, we have listed all compounds with GGA band gaps closest to the experimental values in Tables 1 and 2. Overall, there are 19 0D-OMHHs and 24 1D-OMHHs whose GGA predicted band gaps closely match with experimental values, compared to the entire 56 0D-OMHHs and 54 1D-OMHHs considered in this study. Meanwhile, R2SCAN predicted the closest band gap values for 23 0D-OMHHs and 11 1D-OMHHs compared to experiments, whereas TASK provided the closest predictions for 14 0D-OMHHs and 19 1D-OMHHs. In summary, GGA-predicted band gaps not only show reasonable MAE values but also tend to offer the best predictions of band gaps for the highest number of candidates.

**3.3. Impact of Spin−Orbital Coupling.** Another important setup for band structure calculations is whether to


https://doi.org/10.1021/acs.jpcc.4c05263
J. Phys. Chem. C 2024, 128, 17850−17858

**Table 1. 0D-OMHHs with the GGA Band Gap Being the Closest to Experimental Values**

| conventional name | chemical formula | $E_{Exp}$ (eV) | $E_{GGA}$ (eV) | $E_{R2SCAN}$ (eV) | $E_{TASK}$ (eV) |
|---|---|---|---|---|---|
| $(PBA)_2ZnCl_4$ | $(C_{10}H_{16}N)_2ZnCl_4$ | 4.50[45] | 4.44 | 4.67 | 5.37 |
| $(Bmpip)_2PbBr_4$ | $(C_{10}H_{22}N)_2PbBr_4$ | 3.10[46] | 3.51 | 4.06 | 4.94 |
| $(C_{10}H_{28}N_4)SnI_6{\cdot}4H_2O$ | $(C_{10}H_{28}N_4)SnI_6{\cdot}4H_2O$ | 3.18[47] | 3.26 | 3.51 | 4.44 |
| $(C_{10}H_{28}N_4)SnBr_6{\cdot}4H_2O$ | $(C_{10}H_{28}N_4)SnBr_6{\cdot}4H_2O$ | 3.38[47] | 3.25 | 3.16 | 3.51 |
| $(MTP)_2SbBr_5$ | $(C_{19}H_{18}P)_2SbBr_5$ | 2.27[48] | 2.51 | 2.94 | 3.09 |
| | $(C_{24}H_{20}P)_2ZnBr_4$ | [49] | | | |
| | $(C_{24}H_{20}P)_2ZnCl_2Br_2$ | [49] | | | |
| | $(C_{24}H_{20}P)_2ZnCl_4$ | [49] | | | |
| $(BPA)_2SnCl_6$ | $(C_3H_9BrN)_2SnCl_6$ | 2.97[50] | 2.77 | 3.20 | 3.73 |
| $(C_4N_2H_{14}Br)_4SnBr_6$ | $(C_4N_2H_{14}Br)_4SnBr_6$ | 3.02[13] | 3.47 | 3.77 | 4.72 |
| $(C_4N_2H_{14}Br)_4SnI_6$ | $(C_4N_2H_{14}Br)_4SnI_6$ | 2.48[13] | 2.90 | 3.19 | 3.87 |
| $(1\text{-}mPQBr)_2MnBr_4$ | $(C_5H_{14}N_2Br)_2MnBr_4$ | 2.21[51] | 3.56 | 4.32 | 5.74 |
| $(DPA)_2BiI_9$ | $(C_5H_{16}N_2)_2BiI_9$ | 1.59[52] | 2.00 | 2.10 | 2.62 |
| $(DPA)_3SbCl_6$ | $(C_6H_{16}N)_3SbCl_6$ | 3.07[53] | 3.64 | 3.93 | 4.68 |
| $(C_7H_8N_3)_2SbBr_5$ | $(C_7H_8N_3)_2SbBr_5$ | 2.79[54] | 2.97 | 3.26 | 3.85 |
| $(MXD)_3Bi_2Br_{12}{\cdot}2H_2O$ | $(C_8H_{14}N_2)_3Bi_2Br_{12}{\cdot}2H_2O$ | 2.86[55] | 3.32 | 3.70 | 4.39 |
| $(MXD)BiI_5$ | $(C_8H_{14}N_2)BiI_5$ | 2.15[55] | 2.69 | 3.06 | 3.55 |
| $(DCDA)_3Sb_2Cl_{12}$ | $(C_8H_{20}N_2)_3Sb_2Cl_{12}$ | 3.54[56] | 3.87 | 4.17 | 4.94 |
| $(C_9NH_{20})_2SbCl_5$ | $(C_9NH_{20})_2SbCl_5$ | 2.88[13] | 3.33 | 3.69 | 4.34 |
| $(C_9NH_{20})_2SnBr_4$ | $(C_9NH_{20})_2SnBr_4$ | 2.64[2] | 3.53 | 4.01 | 4.90 |
| $(MA)_4InCl_7$ | $(CH_3NH_3)_4InCl_7$ | 3.34[57] | 3.96 | 4.72 | 5.38 |
| $\alpha\text{-}Gua_3Cu_2I_5$ | $(CH_6N_3)Cu_2I_5$ | 2.80[58] | 2.61 | 3.12 | 3.97 |

**Table 2. 1D-OMHHs with the GGA Band Gap Being the Closest to Experimental Values**

| conventional name | chemical formula | $E_{Exp}$ (eV) | $E_{GGA}$ (eV) | $E_{R2SCAN}$ (eV) | $E_{TASK}$ (eV) |
|---|---|---|---|---|---|
| $BpbmAPb_2I_6$ | $C_{22}H_{42}I_6N_2O_4Pb_2S_4$ | 2.94[59] | 2.77 | 3.11 | 3.44 |
| $[(Me)_2\text{-}DABCO]_2Ag_5Pb_2I_{13}$ | $C_{16}N_4H_{36}Ag_5Pb_2I_{13}$ | 2.33[60] | 2.70 | 2.94 | 3.90 |
| $(DTHPE)_{0.5}PbCl_3$ | $C_{2.5}H_5NPbCl_3$ | 3.83[61] | 3.85 | 4.23 | 4.95 |
| $[DMTHP]PbCl_3$ | $C_6H_{12}N_2PbCl_3$ | 3.77[61] | 3.69 | 4.17 | 4.68 |
| $[H_2DABCO][Ag_2I_4\ (DABCO)]$ | $C_6H_{13}N_2AgI_2$ | 2.84[62] | 2.89 | 3.18 | 4.46 |
| $[DBN]PbCl_3$ | $C_7H_{13}N_2PbCl_3$ | 3.53[61] | 4.13 | 4.43 | 5.32 |
| $[N\text{-}methyldabconium]PbI_3$ | $C_7H_{15}N_2PbI_3$ | 2.92[63] | 3.40 | 3.69 | 4.67 |
| $[(Me)_2\text{-}DABCO]Ag_2PbBr_6$ | $C_8N_2H_{18}Ag_2PbBr_6$ | 2.77[60] | 3.07 | 3.49 | 4.43 |
| CEPbBr | $(ClCH_2CH_2N(CH_3)_3)PbBr_3$ | 3.33[64] | 3.77 | 4.15 | 5.27 |
| $NH_3(CH_3)_6NH_3BiI_5$ | $(C_6H_{13}N)_2BiI_5$ | 2.05[65] | 2.20 | 2.31 | 2.99 |
| $R\bar{3}\text{-}ADP\text{-}SbBr_5$ | $C_5H_{14}Br_5N_2Sb$ | 2.47[66] | 2.51 | 2.71 | 3.30 |
| $R\bar{3}\text{-}HP\text{-}PbBr_3$ | $R\text{-}C_5H_{11}NOPbBr_3$ | 3.29[67] | 3.75 | 4.05 | 5.24 |
| $S\text{-}2\text{-}MPDPbBr_3$ | $S\text{-}C_6H_{13}HPbBr_3$ | 3.51[68] | 3.86 | 4.19 | 5.42 |
| $S\text{-}2\text{-}MPDPbI_3$ | $S\text{-}C_6H_{13}HPbI_3$ | 2.53[68] | 3.38 | 3.67 | 4.72 |
| $S\text{-}MBABiI_4$ | $S\text{-}C_8H_{11}BiI_4N$ | 2.21[69] | 2.69 | 2.88 | 3.53 |
| $TMEDAPb_2Br_6$ | $C_5H_{16}N_2Pb_2Br_6$ | $3 \times 10^{11}$ | 3.33 | 3.69 | 4.82 |
| $(2cepiH)CdCl_3$ | $(C_7H_{15}ClN)CdCl_3$ | 3.35[70] | 4.27 | 5.11 | 6.05 |
| $(2cepyH)PbI_3$ | $(C_6H_{13}Cl_2N)PbI_3$ | 2.75[71] | 3.27 | 3.51 | 4.56 |
| $(C_{12}H_{24}O_6)CsCu_2Br_3$ | $(C_{12}H_{24}O_6)CsCu_2Br_3$ | 1.85[72] | 2.19 | 2.58 | 2.97 |
| $(C_4H_{10}NO)_2SbCl_5$ | $(C_4H_{10}NO)_2SbCl_5$ | 3.25[73] | 3.39 | 3.61 | 4.50 |
| $TMGPbI_3$ | $(C_5H_{13}N_3)PbI_3$ | 3.07[74] | 3.43 | 3.57 | 4.73 |
| $(hep)PbBr_3$ | $(C_7H_{16}N)PbBr_4$ | 3.10[75] | 3.53 | 3.88 | 5.04 |
| $(C_9H_{14}N)SbCl_4$ | $(C_9H_{14}N)SbCl_4$ | 3.47[76] | 3.68 | 4.05 | 4.80 |
| $(Dipa)PbI_3$ | $((CH_3)_2CH)_2NH_2PbI_3$ | 2.64[77] | 3.28 | 3.59 | 4.56 |

consider the relativistic effect through spin−orbital coupling. This can be a relevant effect, especially considering that many OMHHs involve heavy metals such as Pb, Bi, and Sn. The comparison between band gaps predicted by GGA and GGA plus spin−orbital coupling (denoted as GGA+SOC) is presented in Figure 4. The band gap values of GGA and



https://doi.org/10.1021/acs.jpcc.4c05263
J. Phys. Chem. C 2024, 128, 17850−17858

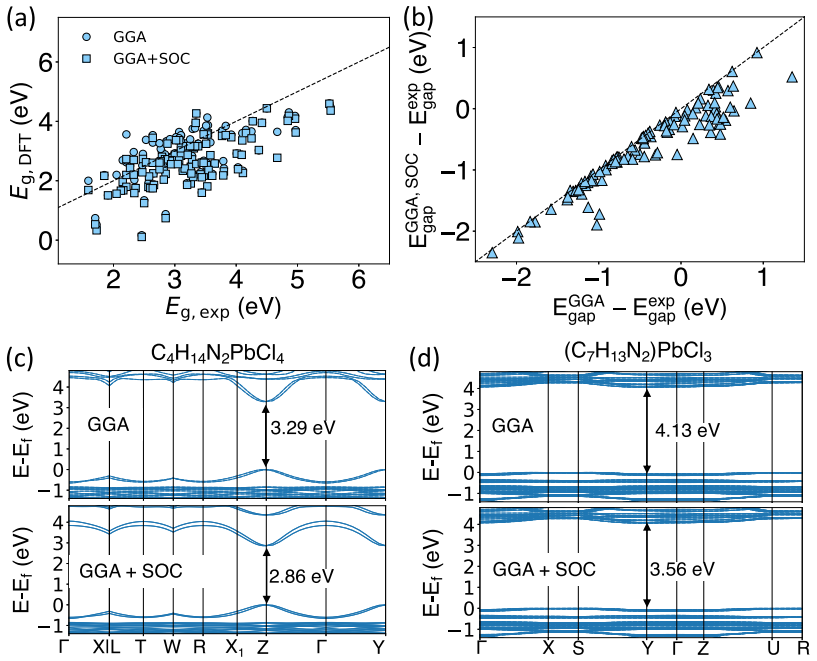


**Figure 4.** (a) Comparison between the GGA-predicted band gap and band gaps predicted by GGA plus spin−orbital coupling (denoted as GGA +SOC); (b) band gap difference of GGA vs experiment and of GGA+SOC vs experiment; (c) band structure of representative compounds of $(C_4H_{14}N_2)PbCl_4$ with better estimation of the band gap by GGA; (d) band structure of representative compounds of $(C_7H_{13}N_2)PbCl_3$ with better estimation of the band gap by GGA+SOC. For (c) and (d), the direct gap used to compare with the optical measurement is illustrated by black arrows.

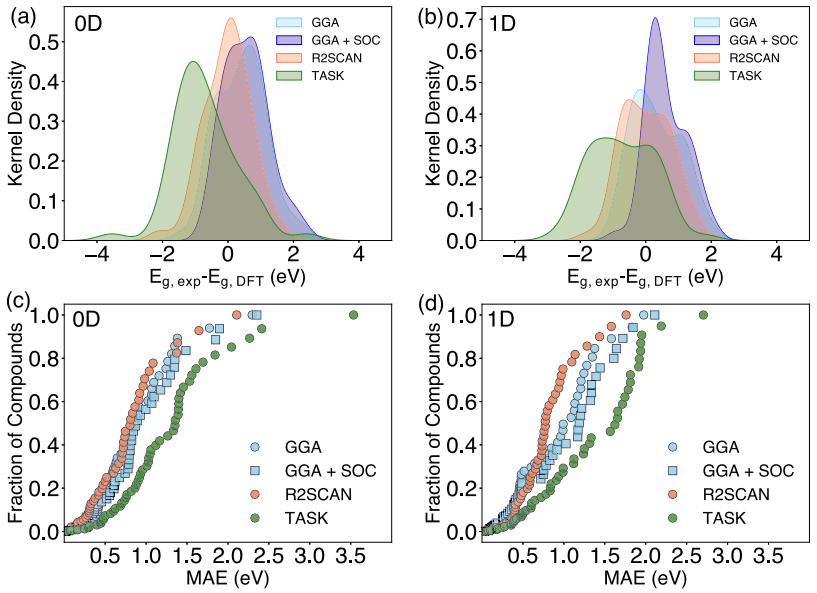


**Figure 5.** Kernel density distributions of (a) 0D- and (b) 1D-OMHHs from GGA, GGA+SOC, R2SCAN, and TASK. The fraction of compounds vs MAE of (c) 0D- and (d) 1D-OMHHs from GGA, GGA+SOC, R2SCAN, and TASK.

GGA+SOC are shown in Tab. S1&Tab. S2. Both 0D- and 1D-OMHH predictions are combined in this plot, given that we did not find any significantly different trends across different dimensionalities. It can be inferred from Figure 4(a) that the general performance between GGA and GGA+SOC is similar. There is no obvious improvement, given that MAEs of GGA and GGA+SOC are 0.66 and 0.67 eV respectively, when calculated for all 0D- and 1D-OMHHs. Moreover, another interesting observation is illustrated in Figure 4(b). It can be inferred that almost all GGA+SOC predictions yield a smaller band gap than GGA by itself. However, this systematic shift of predictions does not necessarily help or hurt the prediction error as it helps the cases when GGA overestimates the band gap, but it will make things worse when GGA underestimates the experimentally measured optical gaps. To illustrate such a "double-edged sword" effect brought by incorporating SOC, we have demonstrated one case when the underestimation brought by SOC deviates further away from the experimental gap (GGA: 3.29 eV, GGA+SOC 2.86 eV, experiment: 3.58 eV) as shown by the calculations of $(C_4H_{14}N_2)PbCl_4$ in Figure 4(c), as well as one case when the lowering of the band gap of $(C_7H_{13}N_2)PbCl_3$ brought by SOC helps get close to the


https://doi.org/10.1021/acs.jpcc.4c05263
J. Phys. Chem. C 2024, 128, 17850−17858

experimental values (GGA: 4.13 eV, GGA+SOC 3.56 eV, experiment: 3.53 eV) (Figure 4(d)).

## 4. DISCUSSION

**4.1. Statistical Trends of Prediction Errors.** Based on the performance analysis of different DFT functionals, we end up with a very interesting observation that GGA turns out to be a suitable choice for predicting the band gap in comparison with GGA+SOC and the two meta-GGA functionals. In the following contexts, we would like to demonstrate a bit more interpretation of the behavior of different functionals and provide more insights into the usage of different functionals for high-throughput screening of electronic structures of OMHHs.

The distributions and statistical features of the prediction errors are demonstrated in Figure 5. Particularly, the kernel density distribution of all four DFT setups for 0D- and 1D-OMHHs is demonstrated in Figures 5(a),(b) respectively. Such distributions will further clarify the fact that, in general, the band gap values predicted by different values follow the order GGA+SOC ≈ GGA < R2SCAN < TASK, which can be roughly estimated from the peak position. Moreover, the fact that the kernel distribution of TASK prediction error centers at ∼1.5 eV indicates that TASK in general tends to overestimate the experimental band gap by 1.5 eV. On the other hand, the distribution of the other three DFT setups will center around 0 eV, indicating much less systematic errors. Moreover, another way of systematically looking at the prediction performance is to plot the fraction of data for specific MAE values, which are demonstrated in Figure 5(c),5(d). It can be seen from these two figures that half of the data sets for both 0D- and 1D-OMHHs can be accurately predicted with MAE values smaller than 0.7 eV using GGA, GGA+SOC, or R2SCAN, which will still be useful for estimating the optical performance as well as electronic conductivity of such materials. On the other hand, TASK tends to mispredict the band gap of almost 80% of candidates with the MAE more than 1 eV. Moreover, even though R2SCAN shows a slightly lower MAE for predicting the experimental band gaps, the difference is marginal, as shown in Figure 5(c),5(d), particularly in the case of predicting 0D-OMHHs.

**4.2. Strategy of Choosing DFT Setups for Predicting the Band Gap.** It seems that there is no perfect way to predict the band gap of OMHHs. However, it is also obvious that it is not necessary to go to the meta-GGA level of theory to improve the accuracy of band gap prediction for matching experimental measurements. Particularly, the computational cost for calculating band gaps using GGA+SOC, R2SCAN, and TASK is demonstrated in Figure 6. All three methods are shown in Figure 6 to cost in general four times more computing resources than GGA. Given the fact that they did not provide an obvious improvement of band gap prediction accuracy, it is fair to suggest that GGA should be sufficient for performing high-throughput screening of OMHHs for obtaining a reasonable estimation of band structures. After the high-throughput screening, a short list of candidates can then be collected for more accurate estimation using more advanced methods, such as hyper-GGA level of theory, random-phase approximation, GW, and Quantum Monte Carlo.

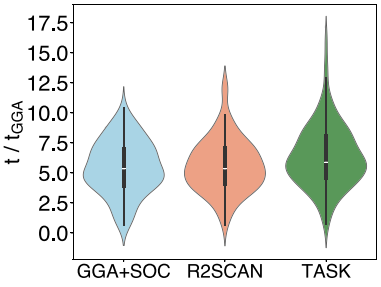


**Figure 6.** Computational cost for calculating band gaps using GGA+SOC, R2SCAN, and TASK compared to GGA.

**4.3. Physical Interpretation.** In addition to prediction accuracy, another important aspect to be considered is why GGA does not show worse performance than other higher-level methods, e.g., GGA+SOC, R2SCAN, and TASK. This is counterintuitive and against the common understanding that semilocal theory such as GGA is generally regarded to underestimate the fundamental band gap.[24] A reasonable hypothesis to understand such behavior is that most of our examined material systems have a strong excitonic effect, which makes the DFT-predicted fundamental band gap larger than the optical band gap measured experimentally from physics. In this case, TASK may demonstrate the correct physics by overestimating the optical band gap, as the DFT results only indicate the value of the fundamental band gap. To provide more evidence of the trend that higher-level DFT theory may still overestimate the band gap, HSE06 calculations for three 0D-OMHH and one 1D-OMHH compounds are presented in Figures S1−S4. It can be seen that HSE06 band gaps are in general the largest or close to the TASK band gap, which is consistent with the argument that TASK is a meta-GGA functional that produces the closest match to hybrid functionals.[22] Moreover, HSE06 also shows bigger errors with experimental band gaps compared to GGA and R2SCAN, which further supports the possibility that the experimental optical band gap may involve a pronounced excitonic effect that intrinsically differs from the Kohn−Sham gap calculated through DFT. However, a comprehensive combination of experimental measurement and higher-level DFT calculations on the excitonic effect will be needed to provide the answer to this puzzle.

It is commonly believed that Kohn−Sham gaps from the GGA functional can be lower than the fundamental gaps, which is defined as the energy difference between ionization energy and electron affinity (I-A).[78,79] Therefore, the GGA functional will also tend to underestimate the experimentally measured optical band gap. Under such situations, higher-level functionals, such as hybrid functionals, tend to offer a closer match to the experimental band gap. However, for the OMHH systems studied in this work, the GGA functional does not show a systematic underestimation of the experimental band gap. On the other hand, meta-GGA, such as TASK, as well as the HSE06 calculations presented in Figures S1−S4, consistently provide a higher band gap than the experimental value. Therefore, the challenge of predicting the optical band gap of OMHH can be fundamentally different from the typical inorganic solids.[78,79] Regardless of the real reason for the discrepancy in band gap prediction from various functionals, our results demonstrate that the optical band gap can be efficiently captured by the GGA level of theory, even if it could be due to a wrong reason. It underscores the effectiveness of using GGA calculations for prescreening good OMHH materials for optoelectronic, electronic, or quantum informa-


https://doi.org/10.1021/acs.jpcc.4c05263
J. Phys. Chem. C 2024, 128, 17850−17858

tion applications, which is a very useful discovery for high-throughput materials screening.

## 5. CONCLUSIONS

In summary, we have presented a systematic evaluation of different DFT functionals, such as GGA, R2SCAN, and TASK, as well as the inclusion of spin−orbital coupling in terms of band gap prediction for 0D- and 1D-OMHHs. The experimental band gaps of 56 0D- and 54 1D-OMHHs are extracted from the literature to serve as the "ground truth" of different DFT functional prediction. Unexpectedly, the accuracy of GGA calculation for OMHHs is comparable to that of R2SCAN or even better than that of TASK. Given that GGA offers a reasonable MAE for predicting all band gaps (e.g., ∼0.65 eV), it can be used as a more practical method for accurate screening of the electronic properties of OMHH systems.

## ■ ASSOCIATED CONTENT

### Supporting Information

The Supporting Information is available free of charge at https://pubs.acs.org/doi/10.1021/acs.jpcc.4c05263.

Band gap of experimental, GGA, GGA+SOC, R2SCAN, and TASK for 0D- and 1D-OMHHs and the band structure of 0D-$(C_6H_{11}N_2)_4Cu_4I_8$, 0D-$(CH_6N_3)Cu_2I_5$, 0D-$(C_8H_{14}N_2)BiI$, and 1D-$C_4N_2H_{14}PbCl_4$ with HSE, GGA, R2SCAN, and TASK functionals (PDF)

## ■ AUTHOR INFORMATION


### Corresponding Authors

**Biwu Ma** − *Department of Chemistry and Biochemistry, Florida State University, Tallahassee, Florida 32304, United States;* orcid.org/0000-0003-1573-8019; Email: bma@fsu.edu

**Bin Ouyang** − *Department of Chemistry and Biochemistry, Florida State University, Tallahassee, Florida 32304, United States;* orcid.org/0000-0002-8181-6815; Email: bouyang@fsu.edu

### Authors

**Yufang He** − *Department of Chemistry and Biochemistry, Florida State University, Tallahassee, Florida 32304, United States*

**Md Sazedul Islam** − *Department of Chemistry and Biochemistry, Florida State University, Tallahassee, Florida 32304, United States*

**Jarek Viera** − *Department of Chemistry and Biochemistry, Florida State University, Tallahassee, Florida 32304, United States*

**Hanwei Gao** − *Department of Physics, Florida State University, Tallahassee, Florida 32304, United States*

**Jianwei Sun** − *Department of Physics and Engineering Physics, Tulane University, New Orleans, Louisiana 70118, United States;* orcid.org/0000-0002-2361-6823

Complete contact information is available at: https://pubs.acs.org/10.1021/acs.jpcc.4c05263


### Notes

The authors declare no competing financial interest.

## ■ ACKNOWLEDGMENTS

Y.H., H.G., and B.O. would like to acknowledge the support from the FSU CRC Seed Grant Program and the startup funding for assistant professor. M.S.I., J.V., and B.M. would like to acknowledge the funding support from the National Science Foundation (NSF) (DMR-2204466). J. Sun acknowledges the support of the U.S. DOE, Office of Science, Basic Energy Sciences, grant No. DE-SC0014208. The computational resources were provided by the Advanced Cyberinfrastructure Coordination Ecosystem: Services & Support (ACCESS), the National Energy Research Scientific Computing Center (NERSC), a DOE Office of Science User Facility supported by the Office of Science and the U.S. Department of Energy under contract no. DE-AC0205CH11231 and the Research Computing Center (RCC) at Florida State University. The computation and data processing were also supported by the supercomputing resources from the Department of Energy's Office of Energy Efficiency and Renewable Energy at the National Renewable Energy Laboratory.

## ■ REFERENCES


(1) Lin, H.; Zhou, C.; Tian, Y.; Siegrist, T.; Ma, B. Low-dimensional organometal halide perovskites. *ACS Energy Lett.* **2018**, *3* (1), 54−62.

(2) Zhou, C.; Lin, H.; Shi, H.; Tian, Y.; Pak, C.; Shatruk, M.; Zhou, Y.; Djurovich, P.; Du, M. H.; Ma, B. A zero-dimensional organic seesaw-shaped tin bromide with highly efficient strongly stokes-shifted deep-red emission. *Angew. Chem.* **2018**, *130* (4), 1033−1036.

(3) Zhou, C.; Tian, Y.; Wang, M.; Rose, A.; Besara, T.; Doyle, N. K.; Yuan, Z.; Wang, J. C.; Clark, R.; Hu, Y.; et al. Low-dimensional organic tin bromide perovskites and their photoinduced structural transformation. *Angew. Chem., Int. Ed.* **2017**, *56* (31), 9018−9022.

(4) Yuan, Z.; Zhou, C.; Tian, Y.; Shu, Y.; Messier, J.; Wang, J. C.; Van De Burgt, L. J.; Kountouriotis, K.; Xin, Y.; Holt, E.; et al. One-dimensional organic lead halide perovskites with efficient bluish white-light emission. *Nat. Commun.* **2017**, *8* (1), No. 14051.

(5) Tan, Z.-K.; Moghaddam, R. S.; Lai, M. L.; Docampo, P.; Higler, R.; Deschler, F.; Price, M.; Sadhanala, A.; Pazos, L. M.; Credgington, D.; et al. Bright light-emitting diodes based on organometal halide perovskite. *Nat. Nanotechnol.* **2014**, *9* (9), 687−692.

(6) Kojima, A.; Teshima, K.; Shirai, Y.; Miyasaka, T. Organometal halide perovskites as visible-light sensitizers for photovoltaic cells. *J. Am. Chem. Soc.* **2009**, *131* (17), 6050−6051.

(7) Xing, G.; Mathews, N.; Lim, S. S.; Yantara, N.; Liu, X.; Sabba, D.; Grätzel, M.; Mhaisalkar, S.; Sum, T. C. Low-temperature solution-processed wavelength-tunable perovskites for lasing. *Nat. Mater.* **2014**, *13* (5), 476−480.

(8) Ling, Y.; Yuan, Z.; Tian, Y.; Wang, X.; Wang, J. C.; Xin, Y.; Hanson, K.; Ma, B.; Gao, H. Bright light-emitting diodes based on organometal halide perovskite nanoplatelets. *Adv. Mater.* **2016**, *28* (2), 305−311.

(9) Worku, M.; Ben-Akacha, A.; Blessed Shonde, T.; Liu, H.; Ma, B. The past, present, and future of metal halide perovskite light-emitting diodes. *Small Sci.* **2021**, *1* (8), No. 2000072.

(10) Zhou, C.; Lin, H.; He, Q.; Xu, L.; Worku, M.; Chaaban, M.; Lee, S.; Shi, X.; Du, M.-H.; Ma, B. Low dimensional metal halide perovskites and hybrids. *Mater. Sci. Eng., R* **2019**, *137*, 38−65.

(11) Lin, H.; Zhou, C.; Neu, J.; Zhou, Y.; Han, D.; Chen, S.; Worku, M.; Chaaban, M.; Lee, S.; Berkwits, E.; et al. Bulk assembly of corrugated 1D metal halides with broadband yellow emission. *Adv. Opt. Mater.* **2019**, *7* (6), No. 1801474.

(12) Huang, J.; Peng, Y.; Jin, J.; Molokeev, M. S.; Yang, X.; Xia, Z. Unveiling white light emission of a one-dimensional Cu (I)-based organometallic halide toward single-phase light-emitting diode applications. *J. Phys. Chem. Lett.* **2021**, *12* (51), 12345−12351.

(13) Zhou, C.; Lin, H.; Tian, Y.; Yuan, Z.; Clark, R.; Chen, B.; van de Burgt, L. J.; Wang, J. C.; Zhou, Y.; Hanson, K.; et al. Luminescent

zero-dimensional organic metal halide hybrids with near-unity quantum efficiency. *Chem. Sci.* **2018**, *9* (3), 586−593.
(14) Zhou, C.; Lin, H.; Lee, S.; Chaaban, M.; Ma, B. Organic−inorganic metal halide hybrids beyond perovskites. *Mater. Res. Lett.* **2018**, *6* (10), 552−569.
(15) Huang, J.; Su, B.; Song, E.; Molokeev, M. S.; Xia, Z. Ultra-broad-band-excitable Cu (I)-based organometallic halide with near-unity emission for light-emitting diode applications. *Chem. Mater.* **2021**, *33* (12), 4382−4389.
(16) Zhou, C.; Xu, L. J.; Lee, S.; Lin, H.; Ma, B. Recent advances in luminescent zero-dimensional organic metal halide hybrids. *Adv. Opt. Mater.* **2021**, *9* (18), No. 2001766.
(17) Kothakonda, M.; Kaplan, A. D.; Isaacs, E. B.; Bartel, C. J.; Furness, J. W.; Ning, J.; Wolverton, C.; Perdew, J. P.; Sun, J. Testing the r2SCAN Density Functional for the Thermodynamic Stability of Solids with and without a van der Waals Correction. *ACS Mater. Au* **2023**, *3* (2), 102−111.
(18) Medvedev, M. G.; Bushmarinov, I. S.; Sun, J.; Perdew, J. P.; Lyssenko, K. A. Density functional theory is straying from the path toward the exact functional. *Science* **2017**, *355* (6320), 49−52.
(19) Peng, H.; Yang, Z.-H.; Perdew, J. P.; Sun, J. Versatile van der Waals density functional based on a meta-generalized gradient approximation. *Phys. Rev. X* **2016**, *6* (4), No. 041005.
(20) Zhang, Y.; Sun, J.; Perdew, J. P.; Wu, X. Comparative first-principles studies of prototypical ferroelectric materials by LDA, GGA, and SCAN meta-GGA. *Phys. Rev. B* **2017**, *96* (3), No. 035143.
(21) Zhang, Y.; Kitchaev, D. A.; Yang, J.; Chen, T.; Dacek, S. T.; Sarmiento-Pérez, R. A.; Marques, M. A. L.; Peng, H.; Ceder, G.; Perdew, J. P.; Sun, J. Efficient first-principles prediction of solid stability: Towards chemical accuracy. *npj Computat. Mater.* **2018**, *4* (1), 9.
(22) Lebeda, T.; Aschebrock, T.; Sun, J.; Leppert, L.; Kümmel, S. Right band gaps for the right reason at low computational cost with a meta-GGA. *Phys. Rev. Mater.* **2023**, *7* (9), No. 093803.
(23) Aschebrock, T.; Kümmel, S. Ultranonlocality and accurate band gaps from a meta-generalized gradient approximation. *Phys. Rev. Res.* **2019**, *1* (3), No. 033082.
(24) Perdew, J. P.; Yang, W.; Burke, K.; Yang, Z.; Gross, E. K.; Scheffler, M.; Scuseria, G. E.; Henderson, T. M.; Zhang, I. Y.; Ruzsinszky, A.; et al. Understanding band gaps of solids in generalized Kohn−Sham theory. *Proc. Natl. Acad. Sci. U.S.A.* **2017**, *114* (11), 2801−2806.
(25) Qiu, D. Y.; Da Jornada, F. H.; Louie, S. G. Optical spectrum of $MoS_2$: many-body effects and diversity of exciton states. *Phys. Rev. Lett.* **2013**, *111* (21), No. 216805.
(26) Hafner, J.; Kresse, G. The vienna ab-initio simulation program VASP: An efficient and versatile tool for studying the structural, dynamic, and electronic properties of materials. In *Properties of Complex Inorganic Solids*; Springer, 1997; pp 69−82.
(27) Perdew, J. P.; Burke, K.; Ernzerhof, M. Generalized gradient approximation made simple. *Phys. Rev. Lett.* **1996**, *77* (18), 3865.
(28) Kresse, G.; Furthmüller, J. Efficient iterative schemes for ab initio total-energy calculations using a plane-wave basis set. *Phys. Rev. B* **1996**, *54* (16), 11169.
(29) Śmiga, S.; Constantin, L. A. Unveiling the physics behind hybrid functionals. *J. Phys. Chem. A* **2020**, *124* (27), 5606−5614.
(30) Arbuznikov, A. V. Hybrid exchange correlation functionals and potentials: Concept elaboration. *J. Struct. Chem.* **2007**, *48*, S1−S31.
(31) Paier, J.; Janesko, B. G.; Henderson, T. M.; Scuseria, G. E.; Grüneis, A.; Kresse, G. Hybrid functionals including random phase approximation correlation and second-order screened exchange. *J. Chem. Phys.* **2010**, *132* (9), No. 094103.
(32) Ceperley, D.; Alder, B. Quantum monte carlo. *Science* **1986**, *231* (4738), 555−560.
(33) Co', G. Introducing the random phase approximation theory. *Universe* **2023**, *9* (3), 141.
(34) Gerosa, M.; Bottani, C.; Di Valentin, C.; Onida, G.; Pacchioni, G. Accuracy of dielectric-dependent hybrid functionals in the prediction of optoelectronic properties of metal oxide semiconductors: a comprehensive comparison with many-body GW and experiments. *J. Phys.: Condens. Matter* **2018**, *30* (4), No. 044003.
(35) Xu, L.-J.; Lin, X.; He, Q.; Worku, M.; Ma, B. Highly efficient eco-friendly X-ray scintillators based on an organic manganese halide. *Nat. Commun.* **2020**, *11* (1), No. 4329.
(36) Jain, A.; Ong, S. P.; Hautier, G.; Chen, W.; Richards, W. D.; Dacek, S.; Cholia, S.; Gunter, D.; Skinner, D.; Ceder, G.; Persson, K. A. Commentary: The Materials Project: A materials genome approach to accelerating materials innovation. *APL Mater.* **2013**, *1* (1), No. 011002.
(37) Sun, J.; Remsing, R. C.; Zhang, Y.; Sun, Z.; Ruzsinszky, A.; Peng, H.; Yang, Z.; Paul, A.; Waghmare, U.; Wu, X.; et al. Accurate first-principles structures and energies of diversely bonded systems from an efficient density functional. *Nat. Chem.* **2016**, *8* (9), 831−836.
(38) Liu, H.; Bai, X.; Ning, J.; Hou, Y.; Song, Z.; Ramasamy, A.; Zhang, R.; Li, Y.; Sun, J.; Xiao, B. Assessing r2SCAN meta-GGA functional for structural parameters, cohesive energy, mechanical modulus, and thermophysical properties of 3d, 4d, and 5d transition metals. *J. Chem. Phys.* **2024**, *160* (2), No. 024102.
(39) Henderson, T. M.; Paier, J.; Scuseria, G. E. Accurate treatment of solids with the HSE screened hybrid. *Phys. Status Solidi (b)* **2011**, *248* (4), 767−774.
(40) Viñes, F.; Lamiel-García, O.; Chul Ko, K.; Yong Lee, J.; Illas, F. Systematic study of the effect of HSE functional internal parameters on the electronic structure and band gap of a representative set of metal oxides. *J. Comput. Chem.* **2017**, *38* (11), 781−789.
(41) Lucero, M. J.; Henderson, T. M.; Scuseria, G. E. Improved semiconductor lattice parameters and band gaps from a middle-range screened hybrid exchange functional. *J. Phys.: Condens. Matter* **2012**, *24* (14), No. 145504.
(42) Henderson, T. M.; Izmaylov, A. F.; Scuseria, G. E.; Savin, A. Assessment of a middle-range hybrid functional. *J. Chem. Theory Comput.* **2008**, *4* (8), 1254−1262.
(43) Yang, Z.-h.; Peng, H.; Sun, J.; Perdew, J. P. More realistic band gaps from meta-generalized gradient approximations: Only in a generalized Kohn-Sham scheme. *Phys. Rev. B* **2016**, *93* (20), No. 205205.
(44) Borlido, P.; Schmidt, J.; Huran, A. W.; Tran, F.; Marques, M. A.; Botti, S. Exchange-correlation functionals for band gaps of solids: benchmark, reparametrization and machine learning. *npj Computat. Mater.* **2020**, *6* (1), 1−17.
(45) He, S.; Hao, S.; Fan, L.; Liu, K.; Cai, C.; Wolverton, C.; Zhao, J.; Liu, Q. Efficient Solar Spectrum-Like White-Light Emission in Zinc-Based Zero-Dimensional Hybrid Metal Halides. *Adv. Opt. Mater.* **2023**, *11* (15), No. 2300218.
(46) Zhang, Z.; Liao, J.-F.; Xing, G. Regulating the coordination geometry of polyhedra in zero-dimensional metal halides for tunable emission. *Nanoscale* **2023**, *15* (11), 5241−5248.
(47) Liu, X.; Li, Y.; Liang, T.; Fan, J. Role of Polyhedron Unit in Distinct Photophysics of Zero-Dimensional Organic−Inorganic Hybrid Tin Halide Compounds. *J. Phys. Chem. Lett.* **2021**, *12* (24), 5765−5773.
(48) Li, B.; Jin, J.; Yin, M.; Zhang, X.; Molokeev, M. S.; Xia, Z.; Xu, Y. Sequential and Reversible Phase Transformations in Zero-Dimensional Organic-Inorganic Hybrid Sb-based Halides towards Multiple Emissions. *Angew. Chem., Int. Ed.* **2022**, *61* (49), No. e202212741.
(49) Xu, L. J.; Plaviak, A.; Lin, X.; Worku, M.; He, Q.; Chaaban, M.; Kim, B. J.; Ma, B. Metal Halide Regulated Photophysical Tuning of Zero-Dimensional Organic Metal Halide Hybrids: From Efficient Phosphorescence to Ultralong Afterglow. *Angew. Chem.* **2020**, *132* (51), 23267−23271.
(50) Teri, G.; Ni, H.-F.; Luo, Q.-F.; Wang, X.-P.; Wang, J.-Q.; Fu, D.-W.; Guo, Q. Tin-based organic−inorganic metal halides with a reversible phase transition and thermochromic response. *Materials Chemistry Frontiers* **2023**, *7* (11), 2235−2240.

(51) Jiang, X.; Chen, Z.; Tao, X. $(1\text{-}C_5H_{14}N_2Br)_2MnBr_4$: A Lead-Free Zero-Dimensional Organic-Metal Halide With Intense Green Photoluminescence. *Front. Chem.* **2020**, *8*, 352.
(52) Wang, Y.; Zhang, S.; Wang, Y.; Yan, J.; Yao, X.; Xu, M.; Lei, X.-w.; Lin, G.; Yue, C.-y. 0D triiodide hybrid halide perovskite for X-ray detection. *Chem. Commun.* **2023**, *59* (60), 9239−9242.
(53) Zhao, J.-Q.; Shi, H.-S.; Zeng, L.-R.; Ge, H.; Hou, Y.-H.; Wu, X.-M.; Yue, C.-Y.; Lei, X.-W. Highly emissive zero-dimensional antimony halide for anti-counterfeiting and confidential information encryption-decryption. *Chem. Eng. J.* **2022**, *431*, No. 134336.
(54) Lin, J.; Liu, K.; Ruan, H.; Sun, N.; Chen, X.; Zhao, J.; Guo, Z.; Liu, Q.; Yuan, W. Zero-dimensional lead-free halide with indirect optical gap and enhanced photoluminescence by Sb doping. *J. Phys. Chem. Lett.* **2022**, *13* (1), 198−207.
(55) Klee, P. S.; Hirano, Y.; Cordes, D. B.; Slawin, A. M.; Payne, J. L. Synthesis, Structure, and Tunability of Zero-Dimensional Organic−Inorganic Metal Halides Utilizing the m-Xylylenediammonium Cation: $MXD_2PbI_6$, $MXDBiI_5$, and $MXD_3Bi_2Br_{12}{\cdot}2H_2O$. *Cryst. Growth Des.* **2022**, *22* (6), 3815−3823.
(56) Chai, C.-Y.; Han, X.-B.; Liu, C.-D.; Fan, C.-C.; Liang, B.-D.; Zhang, W. Circularly polarized luminescence in zero-dimensional antimony halides: structural distortion controlled luminescence thermometer. *J. Phys. Chem. Lett.* **2023**, *14* (17), 4063−4070.
(57) Lin, F.; Yu, G.; Weng, S.; Zhou, C.; Han, Y.; Liu, W.; Zhou, K.; Wang, Y.; Lin, H. Blue photoluminescence enhancement achieved by zero-dimensional organic indium halides via a metal ion doping strategy. *Mater. Chem. Front.* **2022**, *7* (1), 137−144.
(58) Wu, J.; Guo, Y.; Qi, J. L.; Yao, W. D.; Yu, S. X.; Liu, W.; Guo, S. P. Multi-Stimuli Responsive Luminescence and Domino Phase Transition of Hybrid Copper Halides with Nonlinear Optical Switching Behavior. *Angew. Chem.* **2023**, *135* (18), No. e202301937.
(59) Febriansyah, B.; Koh, T. M.; John, R. A.; Ganguly, R.; Li, Y.; Bruno, A.; Mhaisalkar, S. G.; England, J. Inducing panchromatic absorption and photoconductivity in polycrystalline molecular 1D lead-iodide perovskites through $\pi$-stacked viologens. *Chem. Mater.* **2018**, *30* (17), 5827−5830.
(60) Yue, C.-Y.; Sun, C.; Li, D.-Y.; Dong, Y.-H.; Wang, C.-L.; Zhao, H.-F.; Jiang, H.; Jing, Z.-H.; Lei, X.-W. Organic−Inorganic Hybrid Heterometallic Halides with Low-Dimensional Structures and Red Photoluminescence Emissions. *Inorg. Chem.* **2019**, *58* (15), 10304−10312.
(61) Zhang, W.-F.; Pan, W.-J.; Xu, T.; Song, R.-Y.; Zhao, Y.-Y.; Yue, C.-Y.; Lei, X.-W. One-dimensional face-shared perovskites with broadband bluish white-light emissions. *Inorg. Chem.* **2020**, *59* (19), 14085−14092.
(62) Sun, C.; Guo, Y.-H.; Yuan, Y.; Chu, W.-X.; He, W.-L.; Che, H.-X.; Jing, Z.-H.; Yue, C.-Y.; Lei, X.-W. Broadband White-Light Emission in One-Dimensional Organic−Inorganic Hybrid Silver Halide. *Inorg. Chem.* **2020**, *59* (7), 4311−4319.
(63) Xue, C.; Yao, Z.-Y.; Zhang, J.; Liu, W.-L.; Liu, J.-L.; Ren, X.-M. Extra thermo-and water-stable one-dimensional organic−inorganic hybrid perovskite [N-methyldabconium] PbI 3 showing switchable dielectric behaviour, conductivity and bright yellow-green emission. *Chem. Commun.* **2018**, *54* (34), 4321−4324.
(64) Li, D.-F.; Zhao, P.-J.; Deng, X.-H.; Wu, Y.-Z.; He, X.-L.; Liu, D.-S.; Li, Y.-X.; Sui, Y. A new organic−inorganic hybrid perovskite ferroelectric $[ClCH_2CH_2N(CH_3)_3][PbBr_3]$ and Its PVDF matrix-assisted highly-oriented flexible ferroelectric films. *New J. Chem.* **2022**, *46* (40), 19391−19400.
(65) Zhang, W.; Tao, K.; Ji, C.; Sun, Z.; Han, S.; Zhang, J.; Wu, Z.; Luo, J. $(C_6H_{13}N)_2BiI_5$: a one-dimensional lead-free perovskite-derivative photoconductive light absorber. *Inorg. Chem.* **2018**, *57* (8), 4239−4243.
(66) Qi, S.; Cheng, P.; Han, X.; Ge, F.; Shi, R.; Xu, L.; Li, G.; Xu, J. Organic−inorganic hybrid antimony (III) halides for second harmonic generation. *Cryst. Growth Des.* **2022**, *22* (11), 6545−6553.
(67) Peng, X. L.; Han, R. R.; Tang, Y. Z.; Tan, Y. H.; Fan, X. W.; Wang, F. X.; Zhang, H. 1D Chiral Lead Bromide Perovskite with Superior Second-Order Optical Nonlinearity, Photoluminescence, and High-Temperature Reversible Phase Transition. *Chem.−An Asian J.* **2023**, *18* (4), No. e202201206.
(68) Zheng, Y.; Xu, J.; Bu, X. H. 1D Chiral Lead Halide Perovskites with Superior Second-Order Optical Nonlinearity. *Adv. Opt. Mater.* **2022**, *10* (1), No. 2101545.
(69) Yao, L.; Zeng, Z.; Cai, C.; Xu, P.; Gu, H.; Gao, L.; Han, J.; Zhang, X.; Wang, X.; Wang, X.; et al. Strong second-and third-harmonic generation in 1D chiral hybrid bismuth halides. *J. Am. Chem. Soc.* **2021**, *143* (39), 16095−16104.
(70) Qi, Z.; Chen, Y.; Guo, Y.; Yang, X.; Zhang, F.-Q.; Zhou, G.; Zhang, X.-M. Broadband white-light emission in a one-dimensional organic−inorganic hybrid cadmium chloride with face-sharing $CdCl_6$ octahedral chains. *J. Mater. Chem. C* **2021**, *9* (1), 88−94.
(71) Qi, Z.; Gao, H.; Yang, X.; Chen, Y.; Zhang, F.-Q.; Qu, M.; Li, S.-L.; Zhang, X.-M. A One-Dimensional Broadband Emissive Hybrid Lead Iodide with Face-Sharing $PbI_6$ Octahedral Chains. *Inorg. Chem.* **2021**, *60* (20), 15136−15140.
(72) Huang, J.; Peng, Y.; Jin, J.; Molokeev, M. S.; Yang, X.; Xia, Z. Unveiling White Light Emission of a One-Dimensional Cu(I)-Based Organometallic Halide toward Single-Phase Light-Emitting Diode Applications. *J. Phys. Chem. Lett.* **2021**, *12* (51), 12345−12351.
(73) Zhuang, J.-C.; Tan, Y.-H.; Fan, X.-W.; Tang, Y.-Z.; Song, N.; Zhang, Y.-H.; Zhang, H.; Chen, S.-P. A 1D chiral infinite chain organic metal halide hybrid with excellent SHG switching and moderate spontaneous polarization. *New J. Chem.* **2022**, *46* (15), 7103−7107.
(74) Cheng, X.; Yue, S.; Chen, R.; Yin, J.; Cui, B.-B. White Light-Emitting Diodes Based on One-Dimensional Organic−Inorganic Hybrid Metal Chloride with Dual Emission. *Inorg. Chem.* **2022**, *61* (39), 15475−15483.
(75) Mao, L.; Guo, P.; Kepenekian, M.; Hadar, I.; Katan, C.; Even, J.; Schaller, R. D.; Stoumpos, C. C.; Kanatzidis, M. G. Structural Diversity in White-Light-Emitting Hybrid Lead Bromide Perovskites. *J. Am. Chem. Soc.* **2018**, *140* (40), 13078−13088.
(76) Wu, F.; Wei, Q.; Li, X.; Liu, Y.; Huang, W.; Chen, Q.; Li, B.; Luo, J.; Liu, X. Cooperative Enhancement of Second Harmonic Generation in an Organic−Inorganic Hybrid Antimony Halide. *Cryst. Growth Des.* **2022**, *22* (6), 3875−3881.
(77) Maqbool, S.; Thekkayil, Z.; Mandal, P. 1D Diisopropylammonium Lead Iodide Perovskite Shows Exceptional Optical Stability and Third-Order Nonlinearity. *Adv. Opt. Mater.* **2023**, *11* (15), No. 2202942.
(78) Chan, M. K. Y.; Ceder, G. Efficient band gap prediction for solids. *Phys. Rev. Lett.* **2010**, *105* (19), No. 196403.
(79) Baerends, E. J. From the Kohn−Sham band gap to the fundamental gap in solids. An integer electron approach. *Phys. Chem. Chem. Phys.* **2017**, *19* (24), 15639−15656.


https://doi.org/10.1021/acs.jpcc.4c05263
J. Phys. Chem. C 2024, 128, 17850−17858